Catalysis Today 176 (2011) 281–285

Contents lists available at ScienceDirect

Catalysis Today

journal homepage: www.elsevier.com/locate/cattod

NO interaction with bare and transition-metal-ions-doped zirconia

Andrzej Adamski [a,*], Mateusz Tarach [a], Paolo Fornasiero [b], Zbigniew Sojka [a]

[a] Jagiellonian University, Faculty of Chemistry, Ingardena 3, PL 30-060 Cracow, Poland
[b] University of Trieste, Chemistry Department and ICCOM Trieste Research Unit, via L. Giorgieri 1, I 34 127 Trieste, Italy

ARTICLE INFO

Article history:
Received 30 September 2010
Received in revised form 1 December 2010
Accepted 2 December 2010
Available online 7 January 2011

Keywords:
ZrO_2
Doping
Structure
NO adsorption
EPR
TPR

ABSTRACT

Two series of t-ZrO_2 samples doped with 5 mol% of alien Sm, Gd, Mo, Mn and V cations were synthesized by wet impregnation and calcined at 600 °C or 1000 °C for 6 h, respectively. Structural (XRD) and spectroscopic (EPR, RS) characterization was completed by reducibility studies (TPR). Low-temperature NO adsorption, monitored by EPR, was investigated to find the link between structural properties of doped zirconia and activation modes of NO molecules. Relations between the chemical composition and dopant speciation, reducibility of the catalysts and the ways of NO adsorption were elucidated.

1. Introduction

Catalytic removal of noxious nitrogen oxides (NO_x) emitted by both stationary and mobile sources is one of the most important environmental issues [1,2], whereas one of the crucial steps of deNO_x process is activation of NO molecules adsorbed from the gas phase on catalyst surface. On the other hand, adsorption of such reactants is strongly dependent on donor/acceptor properties exhibited by active sites exposed on a given oxide surface, which can be additionally modified by doping with aliovalent transition metal ions (TMIs) [3,4]. The determination of dispersion and oxidation states of TMI-additives is not trivial, because of the heterogeneous character of the solid surface and relatively low concentration of active sites. Therefore it is necessary to study in detail the nature of local electronic interactions between surface sites and the reactant molecules.

It was shown [5], that ZrO_2, which was chosen as a support for a series of our TMI-doped catalysts, exhibit mainly weak Lewis acidity, which can be ascribed to coordinatively unsaturated Zr^{4+} centers produced upon surface dehydroxylation, at which NO can adsorb. Doping of zirconia with transition metal ions can induce strong changes in its adsorbtive behavior toward NO or other redox agents, because the introduced additives bring their intrinsic electronic properties to the system, altering binding affinity to the molecules from the gas phase [6,7].

Due to paramagnetic character of NO molecule and its electron donor/acceptor properties, adsorption of nitric oxide in conjunction with EPR spectroscopy can be used to probe redox functionality of the active sites of oxide catalysts. Additionally, nitric oxide is one of the main reactants of the deNO_x, and investigations of its interaction with catalyst surface remains of vital importance providing hints for better understanding molecular pathways, along which NO can be decomposed or selectively reduced into nitrogen [8,9].

Our aim was to elucidate the effect of additives on the structure and physicochemical properties of zirconia in the context of NO activation. Particular attention is paid to the changes occurring to surface sites during NO adsorption.

2. Experimental

Single-phase tetragonal zirconia of specific surface area 77 m^2/g was synthesized by forced hydrolysis from 0.6 M aqueous solution of $ZrOCl_2 \cdot 8H_2O$ with 25% ammonia solution at room temperature. The fresh precipitate was aged in the parent solution at 100 °C for 48 h under reflux with a periodical supplementation of $NH_{3(aq)}$ in order to keep constant pH 9.3. The resultant zirconia gel was dried at 100 °C for 24 h and calcined in air at 600 °C for 6 h [10,11]. A series of TMI-doped zirconia samples containing 5.0 mol. % of alien additives (Mn^{2+}, Gd^{3+}, Sm^{3+}, V^{5+} and Mo^{6+}) was prepared by wet impregnation of t-ZrO_2 with aqueous solutions of the corresponding salts ($Mn(NO_3)_2$, $Sm(NO_3)_3$, $GdCl_3$, $(NH_4)_6Mo_7O_{24}$, NH_4VO_3). After removal of water, samples were dried at 100 °C for 24 h and calcined in air at 600 or 1000 °C for 6 h. Hereafter the samples of

* Corresponding author. Tel.: +48 12 663 22 24; fax: +48 12 634 05 15.
E-mail address: adamski@chemia.uj.edu.pl (A. Adamski).

0920-5861/$ – see front matter © 2010 Elsevier B.V. All rights reserved.
doi:10.1016/j.cattod.2010.12.011

TMI-doped zirconia will be labelled as 5 M/Zr, where M stands for the guest ion.

XRD measurements were carried out by means of a Philips X'Pert Pro diffractometer using CuK_α radiation, usually in the 2θ range of 10–70° with a 0.02° step. Phase composition of the samples was determined from the following relationship [12]

$$x_m = \frac{I_m(1\,1\,1) + I_m(1\,1\,\bar{1})}{I_m(1\,1\,1) + I_m(1\,1\,\bar{1}) + I_t(1\,1\,1)} \quad \text{and} \quad x_t = 1 - x_m$$

where I_m and I_t stand for intensities of the corresponding monoclinic and tetragonal diffraction peaks. Grain size was evaluated from the Williamson–Hall equation, $B\cos\theta = \lambda/D + 4\varepsilon\sin\theta$, where λ is the wavelenghts, B stands for Bragg maximum halfwidth, D for average grain diameter and ε for average strain.

Raman spectra were collected with a Renishaw InVia spectrometer. The samples were excited with the 785 nm laser and the scattered radiation was collected at 180° with 4 cm^{-1} resolution. The CW-EPR X-band spectra were recorded at room and liquid nitrogen temperature (LNT) with a Bruker ELEXSYS E-500 spectrometer operating at the 100 kHz field modulation. EPR parameters were determined by simulation using the EPRsim32 program [13].

The reducibility of the investigated samples was determined by means of TPR. The experiments were performed using 30 mg of the catalysts, initially pre-treated at 500 °C for 1 h by pulsing O_2 in Ar flow every 75 s. The 5% of H_2/Ar gas mixture was admitted into the reactor and the temperature was ramped (10 °C/min) to 950 °C. The H_2 uptake was monitored using a TCD detector.

NO was adsorbed at the pressure of 10 Torr on the samples outgassed at 350–400 °C for 0.5 h in vacuum ($p \leq 10^{-5}$ Torr). All samples were contacted with gaseous adsorbates at 77 K for 2 min and next exposed to room or elevated temperatures to follow the adsorption progress, monitored by EPR.

3. Results and discussion

3.1. Bulk structure of TMI-doped t-ZrO_2

As it is revealed by XRD measurements (Fig. 1) the phase composition of the investigated catalysts strongly depends on the nature of the introduced transition metal guest ion. In the case of 5 mol% of molybdenum or samarium dopants, the tetragonal zirconia matrix did not exhibit any phase transition after thermal treatment at 600 °C. In the diagnostic region between 25 and 33°a Bragg maximum at 2θ around 30° due to $(1\,1\,1)_T$ reflection can be easily recognized (Fig. 1a–c) [12]. Contrary to this, upon introduction of manganese, gadolinium and especially vanadium ions, the content of tetragonal phase in the calcined catalysts decreased to 60%–80%, respectively (*cf.* insert to Fig. 1), as it can be deduced from the intensity of two new $(1\,1\,\bar{1})_M$ and $(1\,1\,1)_M$ reflections at 2θ of 28 and 32°, characteristic of the monoclinic polymorph (m-ZrO_2) (Fig. 1d–f). As the calcination temperature was rather low in comparison to the Tammann temperature of ZrO_2 (T_t = 800–1350 °C), defined as $T_t = (0.3–0.5)T_m$ [14], where T_m = 2700 °C is the melting point of ZrO_2, one cannot expect any significant migration of the alien ions into the bulk of zirconia and the resultant phase composition changes. Only in the case of V^{4+} ions exhibiting the lowest difference (~14%) in the cationic size with respect to Zr^{4+} ions [15], such possibility is realistic and has been evidenced experimentally [16]. Indeed, the content of m-ZrO_2 was found to be the highest in the case of 5V/Zr. More detailed account of t-ZrO_2 metastabilization has been discussed elsewhere [10,11]. Stabilization of the t-ZrO_2 phase is strongly related to the surface energy and the size of the grains, which can be modified by the presence of dopants, in agreement with the trends shown in the insert to Fig. 1, where

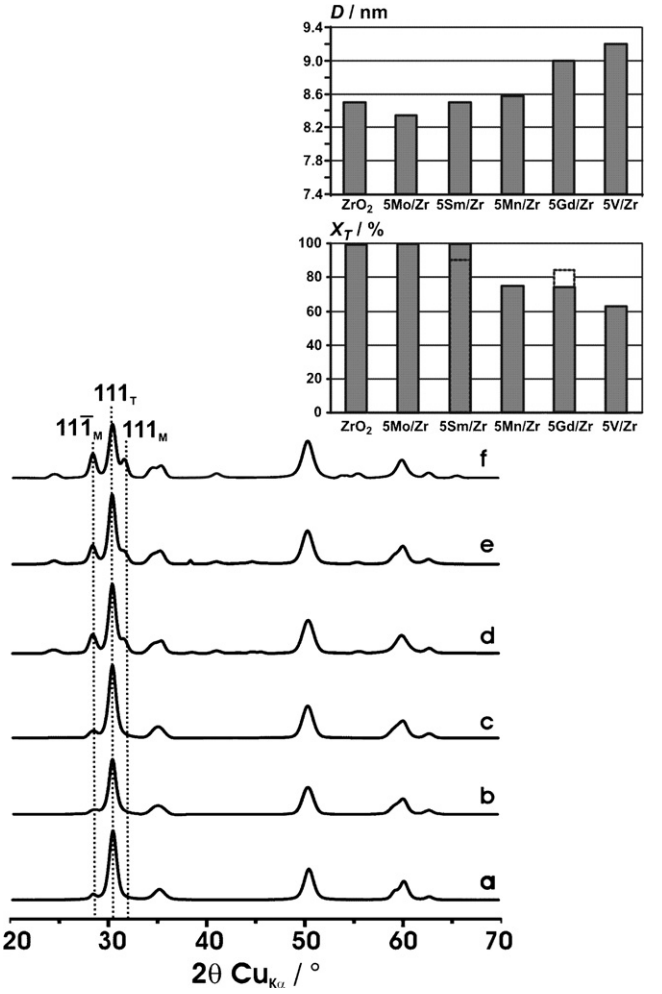

Fig. 1. XRD patterns of 5TMI/Zr samples calcined at 600 °C: (a) parent ZrO_2, (b) 5Mo/Zr, (c) 5Sm/Zr, (d) 5Mn/Zr, (e) 5Gd/Zr and (f) 5V/Zr. In the insert, content of tetragonal phase (X_T) (dashed line for 1000 °C) and corresponding grain size (D) evolution is shown.

decrease of the t-ZrO_2 content in Mn-, Gd- and V-doped samples is accompanied with simultaneous increase of the grain size. Such correlation was even more pronounced in the case of Mn-, V- and Mo-doped samples calcined at 1000 °C, as the zirconia matrix was essentially monoclinic in this case, whereas for 5Gd/Zr and 5Sm/Zr samples the phase composition was modified by 6.0–10.0% merely (Fig. 1 insert, dashed line). In parallel, the grain size D increased from 8.5 to 9.2 nm for 5Mn/Zr, 5Mo/Zr and 5Mo/Zr samples calcined at 600 °C to 42.2–56.0 nm for these samples calcined at 1000 °C. Sintering effect was weakly pronounced for two remaining 5Gd/Zr and 5Sm/Zr samples, for which the D value increased from 8.5–9.0 nm to 12.3–12.9 nm.

Similarly to XRD results, presence of the additives is not revealed in the Raman spectra of the samples calcined at 600 °C (Fig. 2). One can notice only, that all reported spectra are characteristic of tetragonal ZrO_2 (see insert in Fig. 2). The factor group analysis predicts 6 ($A_{1g} + 2B_{1g} + 3E_g$) Raman-active modes for tetragonal polymorph and 18 ($9A_g + 9B_g$) for monoclinic one [17,18]. Just the most intensive bands between 465 and 490 cm^{-1} typical of t-ZrO_2 which dominated the spectra can be attributed to the symmetrical mode of the fluorite-like structure and the bands at ~170 and 310 cm^{-1} along with an additional broad feature centered at ~635 cm^{-1} confirm the presence of a pseudo-cubic tetragonal phase. Only in the spectrum of 5V/Zr two badly resolved lines just above 350 cm^{-1} can originate from m-ZrO_2. It is not surprising that not all lines

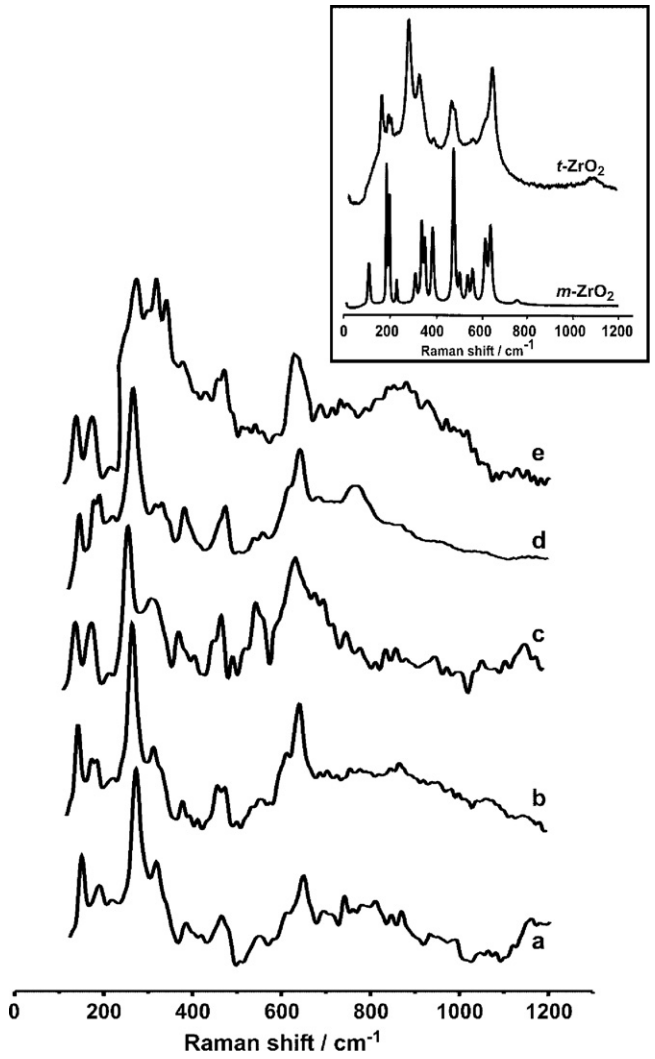

Fig. 2. Raman spectra of the catalysts calcined at 600 °C: (a) 5Mo/Zr, (b) 5Sm/Zr, (c) 5Mn/Zr, (d) 5Gd/Zr and (e) 5V/Zr. In the insert, RS spectra of m- and t-ZrO_2 single phases are shown [11].

postulated by factor group analysis for m-ZrO_2 are simultaneously observed in this spectrum (Fig. 2e). Even in the spectrum of m-ZrO_2 single phase all 18 modes can be observed very seldom. In the case of 5V/Zr sample the situation is even more complicated due to coexistence of two phases t-ZrO_2 and m-ZrO_2. Overlapping of the Raman bands characteristic of the monoclinic polymorph with those, ascribed to t-ZrO_2, of higher intensity and much broader in comparison to the bands of m-ZrO_2, make only a few diagnostic lines of monoclinic zirconia to be visible. Raman results along with XRD, show that t-ZrO_2 polymorph is the predominant component of all TMI-doped samples calcined at 600 °C.

3.2. Status of TMI sites and their reducibility

Introduction of the dopants by impregnation followed by calcination in air of the samples has two preparative consequences, a relatively weak dispersion of the heterogenically deposited ions on t-ZrO_2 surface and possible changes in their oxidation states. As indicated by EPR measurements, for a series of the investigated samples calcined at 600 °C, both oxidation and reduction of the dopants can occur in the individual cases. Vanadium (V) ions were partially reduced to the paramagnetic V(IV), giving rise to the spectrum presented in Fig. 3A-a, with the characteristic well resolved hyperfine structure originating from interaction of an unpaired electron with ^{51}V nucleus ($I = 7/2$, 99.76%). Computer simulations revealed, that both surface and bulk isolated V^{4+} ions as well as magnetically interacting vanadium centers contributed to this spectrum of 5V/Zr. Detailed values of the obtained EPR parameters were close to those reported elsewhere [19]. Two factors controls the process of V(IV) formation: the concentration of ammonia liberated during NH_4VO_3 decomposition and the temperature. In a similar way Mo(VI) was partially reduced to Mo(V), revealed by characteristic EPR signal at $g_{av} = 1.93$ with weak hyperfine structure due to ^{95}Mo and ^{97}Mo nuclei with $I = 5/2$ and 25% of total abundance (Fig. 3A-b) [20]. In turn, Mn(II) ions were most probably oxidized to Mn(III)/Mn(IV) species [21], responsible for complex spectrum centered around $g = 2.01$ (Fig. 3A-c).

Information about speciation of the dopant ions in the investigated samples provided by EPR can be completed by TPR studies (Fig. 4). Such speciation is directly related to redox properties of the additives and, therefore, can be characterized by reducibility measurements, however due to multistep reduction and overlapping maxima on our TPR profiles obtained information is sometimes not precise enough. The t-ZrO_2 support, 5Gd/Zr and 5Sm/Zr calcined at 600 and 1000 °C were stable below 950 °C (Fig. 4AB a–c) Contrary to this, the other samples: 5Mn/Zr, 5Mo/Zr and 5V/Zr underwent stepwise reduction, as it can be inferred from the presence of several maxima visible in the corresponding thermograms (Fig. 4AB d–f). The Mn-containing samples calcined at 600 and 1000 °C exhibited broad reduction band, typical of several reduction steps. H_2 consumption maxima visible between 190 and 470 °C in the case of 5Mn/Zr calcined at 600 °C, were shifted up to 440–790 °C (with a predominant maximum at 740 °C) after calcination of at 1000 °C (Fig. 4AB-d). Taking into account the variety of possible stoichiometric and non-stoichiometric oxomanganese species and multiplicity of the oxidation states (II–IV) occurring on catalyst surface, precise attribution of the observed maxima is rather difficult. Original oxidation state of manganese cations calculated based on H_2 uptake was about 4 (H/Mn = 3.82). It is however clear, that the shift to higher temperatures, observed in Fig. 4B-d in comparison to that in Fig. 4A-d resulted from strong sintering of the catalyst grains calcined at 1000 °C. This can be related with the formation of three dimensional (3D) Mn_xO_y forms, which are apparently less reducible. Similar effects were observed also for 5V/Zr and 5Mo/Zr samples calcined at 1000 °C. It is noteworthy, that in the case of samples calcined at 1000 °C hydrogen consumption was lower by 32–46% in comparison to that obtained for samples calcined at 600 °C. Such effect can be explained by a partial loss of active phase from catalysts surface. However, high-temperature EPR spectra confirmed that in all cases described above at least a part of the thermally resistant TMIs was still present after thermal treatment at 1000 °C. In the case of both TPR profiles for 5Mo/Zr samples a maximum around 440 °C can be attributed to the mild reduction of the octahedral molybdenum, possibly to the mixed-valence Mo_4O_{11}-like structures [22]. TPR maxima appearing for 5Mo/Zr calcined at 600 °C at higher temperatures (850 °C) were shifted down to 680 °C for sample calcined at 1000 °C. These maxima can be related to direct reduction of Mo(VI) to Mo(IV) in various surface oxospecies, similar to nanocrystalline MoO_3 [22,23]. A high-temperature maximum visible in both thermograms at 950 °C is usually attributed to the reduction of MoO_2 to the metallic molybdenum (H/Mo = 5.12) [20]. The TPR profile obtained for 5V/Zr calcined at 600 °C was dominated by an intense maximum at 460 °C, which was characteristic of the reduction of surface VO_x oligospecies (Fig. 4A-f). Next weak maximum at 600–620 °C was observed for 5V/Zr calcined at both 600 and 1000 °C (Fig. 4B-f). Such temperature was slightly below the range typical of nanocrystalline V_2O_5 reduction (660–690 °C) [24,25]. Most probably an intermediate V_xO_y form, structurally close to crystalline V_2O_5, was reduced in these tem-

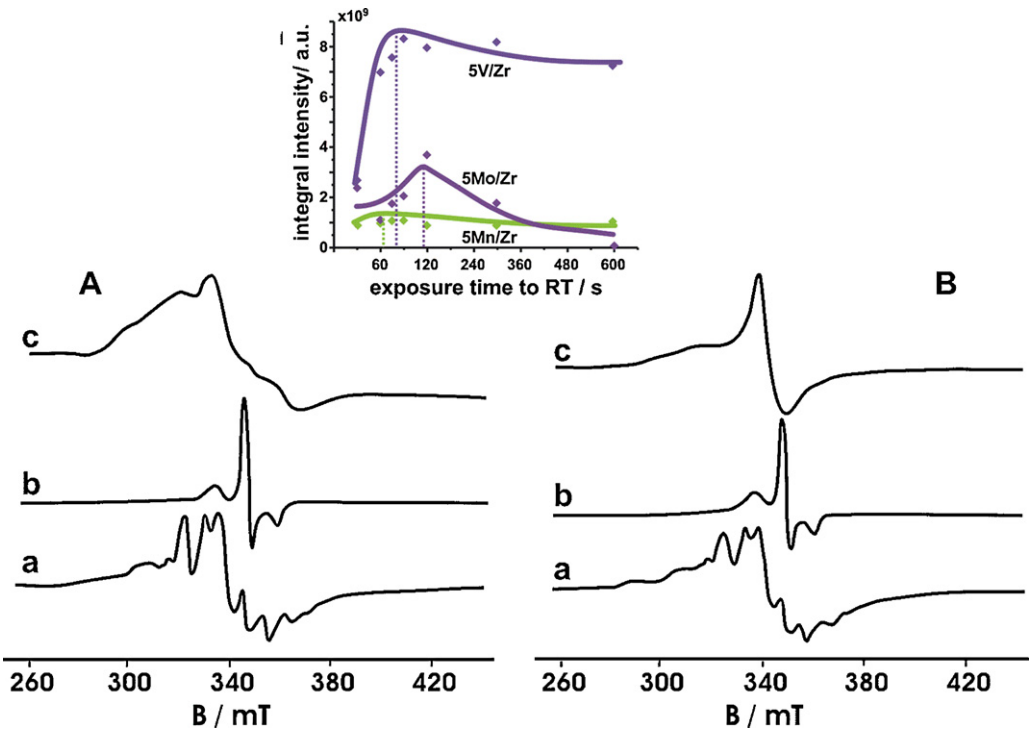

Fig. 3. EPR spectra of 5TMI/Zr samples (A) before NO adsorption: (a) 5V/Zr; (b) 5Mo/Zr; (c) 5Mn/Zr and (B) corresponding EPR spectra after adsorption of NO (p_{NO} = 10 Torr) at LNT and after subsequent 10 min exposure to RT. In the insert, evolution of the EPR spectra intensity as a function of the time of exposure to RT.

perature range (H/V = 4.32). As the high-temperature maximum appeared for 5V/Zr calcined at 1000 °C and it was practically absent in the case of the sample calcined at 600 °C, segregation of vanadium species into 3D structures is postulated to be responsible for its appearence.

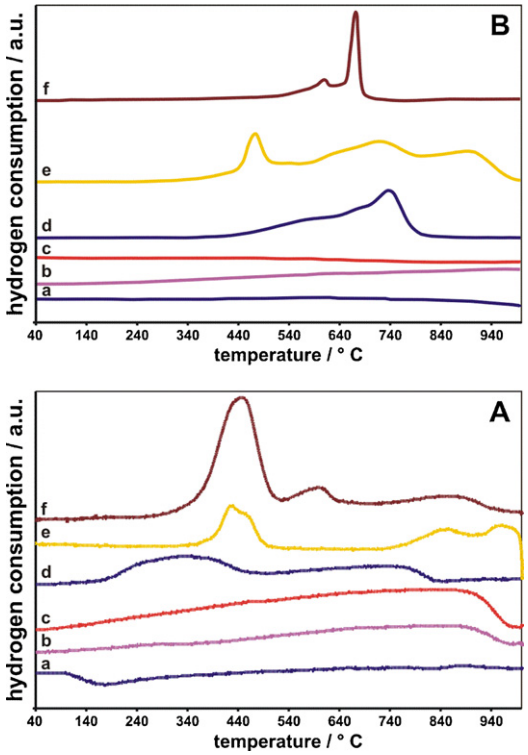

Fig. 4. TPR profiles of 5TMI/Zr samples calcined at 600 °C (A) and 1000 °C (B): (a) parent ZrO_2; (b) 5Gd/Zr; (c) 5Sm/Zr; (d) 5Mn/Zr; (e) 5Mo/Zr; (f) 5V/Zr.

3.3. NO adsorption

Adsorption of 10 Torr of nitric oxide on the bare t-ZrO_2 at 77 K resulted in the formation of $\{Zr\text{-}NO\}^1$ surface mononitrosyls, as it can be inferred from the presence of the well resolved three line hyperfine structure due to the interaction of the unpaired electron with ^{14}N nucleus (I = 1, 99.6%) in the EPR spectrum [26]. Such signal was, however, not observed for TMI-doped samples, because of the overlapping with much more intense signals from the paramagnetic V^{4+}, Mo^{5+}, and Mn^{x+} ions or from their adducts with the adsorbed NO (Fig. 3B a–c). Three cases can be distinguished here: (i) NO physisorption (5Gd/Zr and 5Sm/Zr), (ii) weak chemisorption without electron transfer (5Mn/Zr) and (iii) reductive adsorption – (5Mo/Zr and 5V/Zr). Any specific type of NO adsorption on surface centers of non-reductive samples was observed (5Gd/Zr and 5Sm/Zr). Just traces of the signal at $g \approx 2.0$ attributable to weakly physisorbed NO molecules were observed in a few EPR spectra of 5Sm/Zr sample. Surprisingly, also in the case of Mn-doped zirconia only the signal from weakly chemisorbed NO dominated at 77 K (Fig. 3B-c). The EPR signal was in this case distinctly broader and the hyperfine structure was practically not resolved, mainly due to averaging caused by the motion of weakly bound NO molecules. Contrary to this, the low-temperature contact of the 5Mo/Zr and 5V/Zr catalysts calcined at 600 °C with 10 Torr of NO led to distinct changes in the intensities of the EPR spectra (Fig. 3B-a and b). This means that the adsorbed NO was consumed during the reaction with the surface TMI. An increase in the intensity of the EPR signals attributed to Mo^{5+} and V^{4+} ions just after NO introduction at 77 K and exposure of the samples to room temperature was stronger in the case of 5V/Zr sample (Fig. 3 insert). The observed effects can be explained by the progressive reduction of V(V) and Mo(VI) centers by the ligated NO *via* ligand to metal electron-transfer (LMET) according to the equations:

$$NO\,(^2\Pi_{1/2}) + Mo^{6+}\,(\text{surface}) = \eta^1\text{-}\{Mo^{5+}\text{–}NO\}^1$$

$$NO(^2\Pi_{1/2}) + V^{5+}(\text{surface}) = \eta^1\text{-}\{V^{4+}\text{–}NO\}^1$$

The exposure of the these complexes to the room temperature for more than 4 min resulted in the progressive decrease in the intensity of the EPR signals associated with the Mo^{5+}–NO and V^{4+}–NO magnetophors (Fig. 3), possibly due to the further interaction with gaseous NO *via* spin-pairing mechanism or further reduction of TMI sites. Earlier IR experiments confirmed that low-temperature (−120 °C) adsorption of 5–10 Torr of NO on 5Mo/Zr and 5V/Zr followed by exposure of the samples to temperature resulted in the formation of the surface nitrates of bridging and chelating structure [20].

4. Conclusions

Structural characterization of two series of zirconia samples doped with 5 mol% of TMI, synthesized by impregnation and calcined at 600 and 1000 °C have been performed. Positive effect of molybdenum and samarium doping on metastabilization of tetragonal zirconia was confirmed. Contrary to this, in the case of vanadium-doped systems calcined at 600 °C, the content of t-ZrO_2 dropped to 60%, suggesting rather surface than bulk effect of TMI-doping.

Speciation of paramagnetic ions and the reducibility of TMI-doped zirconia were strongly dependent on the nature of the introduced dopant. Reducible samples of molybdenum-, manganese- and vanadium-ions-doped zirconia exhibited reach heterogeneity of surface architecture including diversity of possible oxidation states. On the basis of EPR results, three possible situations observed after low-temperature NO adsorption can be distinguished: (i) NO physisorption (5Gd/Zr and 5Sm/Zr), (ii) weak chemisorption without electron transfer (5Mn/Zr), and (iii) reductive adsorption (5Mo/Zr and 5V/Zr). Electron transfer from the NO ligand to metal center leads to the progressive reduction of surface TMI sites with simultaneous NO oxidation.

Acknowledgements

Authors are grateful to Professor A. Wesełucha-Birczyńska from Faculty of Chemistry of the Jagiellonian University for recording the Raman spectra and to Mr. M. Cargnello (B.Sc.) from Department of Chemical Sciences, University of Trieste for the TPR results.

The work was financially supported by the Polish Ministry of Science and Higher Education within the international research project No. DWM/N112/COST/2008. The research was partially carried out with the equipment purchased thanks to the financial support of the European Regional Development Fund in the framework of the Polish Innovation Economy Operational Program (contract no. POIG.02.01.00-12-023/08).

References

[1] J.N. Armor, in: J.N. Armor (Ed.), Enivironmental Catalysis, ASC Symp. Series, vol. 552, ACS, Washington, 1994.
[2] P. Forzatti, Appl. Catal. A 222 (2001) 221.
[3] Z. Sojka, P. Jakubus, A. Adamski, A. Kotarba, Key Eng. Mater. 253 (2003) 129.
[4] D. Yang, J. Li, M. Wen, C. Song, Catal. Today 139 (2008) 2.
[5] C. Morterra, E. Giamello, L. Orio, M. Volante, J. Phys. Chem. 94 (1990) 3111.
[6] J.A. Rodriguez, M. Pérez, T. Jirsak, L. González, A. Maiti, J.L. Larese, J. Phys. Chem. B 105 (2001) 5497.
[7] Y. Toda, T. Ohno, F. Hatayama, H. Myiata, Appl. Catal. A 207 (2001) 273.
[8] A. Gutsze, M. Plato, H.G. Karge, F. Witzel, J. Chem. Soc., Faraday Trans. 92 (1996) 2495.
[9] A. Volodin, D. Biglino, Y. Itagaki, M. Shiotani, A. Lund, Chem. Phys. Lett. 327 (2000) 165.
[10] P. Jakubus, A. Adamski, M. Kurzawa, Z. Sojka, J. Therm. Anal. Calorim. 72 (2003) 299.
[11] A. Adamski, P. Jakubus, Z. Sojka, Nukleonika 51 (Suppl. 1) (2006) S27.
[12] P.D.L. Mercera, J.G. van Ommen, E.B.M. Doesburg, A.J. Burggraaf, J.R.H. Ross, Appl. Catal. 71 (1991) 363.
[13] T. Spalek, P. Pietrzyk, Z. Sojka, J. Chem. Inf. Model 45 (2005) 18.
[14] G. Tammann, Q.A. Mansuri, Z. Allg. Chem. 126 (1923) 119.
[15] R.D. Shannon, Acta Crystalogr. A 32 (1976) 751.
[16] A. Adamski, Z. Sojka, K. Dyrek, M. Che, Solid State Ionics 117 (1999) 113.
[17] T. Hirata, E. Asari, M. Kitajima, J. Solid State Chem. 110 (1994) 201.
[18] V. Sánchez-Escribano, E. Fernández-López, M. Panizza, C. Resini, J.-M. Gallardo-Amores, G. Busca, Solid State Sci. 5 (2003) 1369.
[19] A. Adamski, T. Spałek, Z. Sojka, Res. Chem. Intermed. 29 (2003) 793.
[20] A. Adamski, P. Zapała, P. Jakubus, Z. Sojka, Top. Catal. 52 (2009) 993.
[21] W.C. Las, D. Gouvea, W. Sano, Solid State Sci. 1 (1999) 331.
[22] T. Baskar, K.R. Reddy, C.P. Kumar, M.R.V.S. Murthy, K.V.R. Cahry, Appl. Catal. A 211 (2001) 189.
[23] C. Kenney, Y. Maham, A.E. Nelson, Thermochim. Acta 434 (2005) 55.
[24] S. Albrecht, G. Wendt, G. Lippold, A. Adamski, K. Dyrek, Solid State Ionics 101–103 (1997) 909.
[25] A. Adamski, Z. Sojka, K. Dyrek, M. Che, G. Wendt, S. Albrecht, Langmuir 15 (1999) 5733.
[26] A. Adamski, P. Zapała, L. Chmielarz, J.A.J. Rodriguez, G. Djéga-Mariadassou, Z. Sojka, Catal. Today, this issue, doi:10.1016/j.cattod.2010.11.076.